CO12-1 Isotope Dilution-Neutron Activation Analysis for Quantifying Hafnium

T. Takatsuka, K. Hirata, Y. Iinuma[1], R. Okumura[1],
H. Yoshinaga, and K. Takamiya[1]

National Metrology Institute of Japan, National Institute of Advanced Industrial Science and Technology
[1]Institute for Integrated Radiation and Nuclear Science, Kyoto University

INTRODUCTION: Hafnium (Hf) oxide is utilized as high-*k* dielectric films for semiconductor devices especially with fast and low-power operation. Additionally, the films are being introduced as ferroelectric material on ferroelectric transistors and memories. The device fabrication process should be precisely controlled for such dielectric films. We aimed to quantify Hf in Hf oxide films in weight unit by means of isotope dilution-neutron activation analysis (ID-NAA) [1].

EXPERIMENTS: Hf oxide films were deposited on 4-inch Si wafers by magnetron sputtering. The target thickness was set to 4 nm. The prepared wafers with the films were cut into 10 mm × 10 mm pieces for the measurements.

The procedure for ID-NAA has two sequences of an isotope dilution (ID) and a reverse-ID to ensure traceability to the SI units; the latter sequence was performed to determine the Hf concentration in a spike solution by referring to a Hf standard. The spike solution was prepared by dissolving ^{174}Hf-enriched Hf oxide (Oak Ridge) in a HNO_3 + HF aqueous solution, and by diluting to a proper concentration. For calibrating the amounts of Hf, a working standard solution was prepared by diluting NIST SRM 3122 gravimetrically. For the ID analysis, small amount of the spike solution was dropped onto each Hf oxide sample (HfO_2+Sp), while the spike solution or standard solution was dropped separately onto each piece of cleaned filter paper (Sp or STD), as shown in Fig. 1. For the reverse-ID analysis, the spike and standard solutions were dropped onto one piece of filter paper (Sp+STD).

For validation, the Hf concentration of the spike solution was also determined by NAA with internal standards. Four concentration levels of working standard solutions were prepared; an internal standard solution of Sb from NIST SRM 3102, three Hf and Sb mixed standard solutions with different Hf concentrations for the calibration. For the quantification of the spike solution, the specimens were prepared using the spike solution before diluting since the diluted spike solution has little Hf-180 to be quantified. Weighed portion of the spike solution was dropped onto a filter paper followed by dropping the Sb standard. As for standards, aliquots of the working standard solutions of Hf and Sb mixture were weighed and dropped onto filter papers.

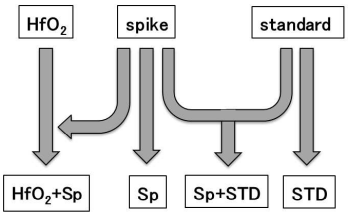

Fig. 1. Sample preparation for ID-NAA.

All the samples were sealed up separately in clean polyethylene bags, followed by being stacked in a polyethylene container for the neutron irradiation. The irradiation was performed for 4 hours with a 5.5×10^{12} cm^{-2}·s^{-1} thermal neutron fluence rate at Pn-2 in the Kyoto university research reactor (KUR). The gamma-ray activity of each sample was measured by a high-purity germanium detector (CANBERRA).

RESULTS: From the gamma-ray spectrum, the gamma-ray intensity ratio of ^{175}Hf to ^{181}Hf and ^{181}Hf to ^{124}Sb were calculated for ID and internal standard method, respectively. The Hf concentration in a spike solution was determined to be 6.63 mg/kg by reverse-ID. The amounts of Hf in the Hf oxide samples were calculated from the intensity ratios based on a formula reported in Ref. 1. Dividing the Hf amounts by measured sample surface areas, the area densities were calculated to be 3.64 μg·cm^{-2} and 3.63 μg·cm^{-2} for two measured samples. From the calibration curve by internal standard method in Fig. 2, the spike concentration was determined to be 108 mg/kg. For comparison, the determined spike concentrations were converted into the relative ones to the nominal concentrations since the nominal concentrations were different from each other. The resultant relative concentrations were 0.982 and 0.978 for reverse-ID and internal stand method, respectively. This agreement showed the reverse-ID procedure in ID-NAA was appropriate for the quantification.

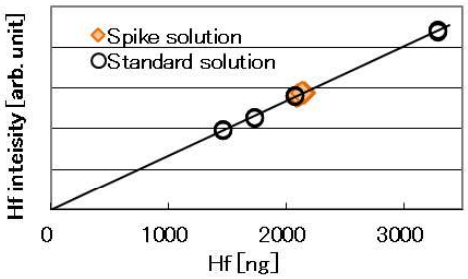

Fig. 2. Calibration curve for determining the spike concentration by the internal standard method.

REFERENCES:

[1] C. Yonezawa *et al.*, Anal. Chem., **55** (1983) 2059-2062.

CO12-2 Study on Superposition of Terahertz Coherent Radiation Using a Ring Resonator

N. Sei and T. Takahashi[1]

Research Institute for Measurement and Analytical Instrumentation, National Institute of Advanced Industrial Science and Technology

[1]Institute for Integrated Radiation and Nuclear Science, Kyoto University

INTRODUCTION: Research on nonlinear spectroscopy has been explored in the terahertz (THz) region where low-energy excitations and photoinduced phase transitions can be observed, and developments of broadband THz light sources with high peak power have been desired [1]. A short-pulse relativistic electron beam is suitable for generating coherent radiation in the THz region, and THz light sources and their applications have been developed in a lot of accelerator facilities [2]. As coherent Cherenkov radiation matched to a circular plane wave, which was demonstrated in our past joint research [3], a method for extracting high-power THz light from the relativistic electron beam by devising a principle of light emission has been mainly studied. Although the development of a new high-efficiency principle of light emission was important factor for realizing high-power THz light, this approach alone was not enough.

Therefore, we proposed that coherent radiation generated by a pulse train of electron bunches was confined in a ring resonator and superimposed with the same phase. We succeeded in observing THz light pulses extracted from a ring resonator in an L-band linac at Kyoto University Institute for Integrated Radiation and Nuclear Science (KURNS-LINAC).

EXPERIMENTS: The experiments were performed using an electron beam with the energy of 42 MeV and the macropulse duration of 47 ns. The reputation frequency of the macropulse of the electron beam was 30 Hz. Figure 1 shows a photograph of the ring resonator used in the experiments. A hollow aluminum cylindrical tube with an inner diameter of 17.5 mm was installed as a collimator upstream the ring resonator. The electron beam passing through the collimator injected to a hole with a diameter of 5 mm on an aluminum thin foil and generated coherent forward diffraction radiation in the ring resonator. Furthermore, the electron beam passed through an aluminum thin foil and generated coherent backward transition radiation. The current of the electron beam passed through another aluminum thin foil was approximately 60 μA. These aluminum thin foils were also used as mirrors constituting the ring resonator. The two coherent radiations were confined in the ring resonator composed of four mirrors, which included two parabolic mirrors with the focal length of 508 mm. The length of the resonator was 922 mm, which was four times the interval of the electron bunches. A part of the resonant light was extracted from the resonator through the hole formed in the aluminum thin foil and transported to an experimental room. The transported resonant light was detected by a D-band diode detector (Millitech Inc., DXP-06), and the output power was measured by an oscilloscope with the frequency band less than 350 GHz.

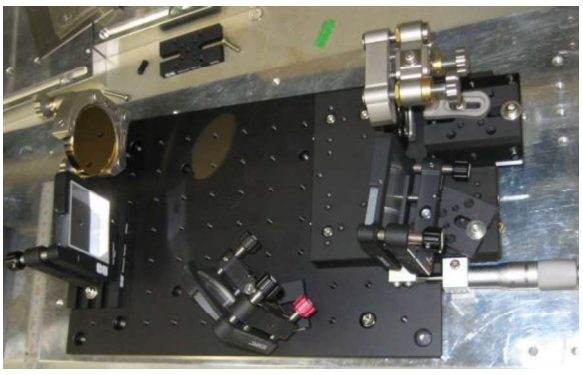

Fig. 1. Photograph of the ring resonator.

RESULTS: Figure 2 shows a macropulse of the THz-light power measured by the D-band diode detector. Although the temporal resolution of the measured THz-light power was insufficient due to the low frequency band of the oscilloscope, it was found that the detector could identified coherent radiation generated by each electron bunch. By using an oscilloscope with a wider band, it will be possible to observe the micropulse waveform of the resonant THz light and to adjust the length of the resonator. We also plan to extract the THz light from the resonator using a thin film which hardly absorbs light in the THz region.

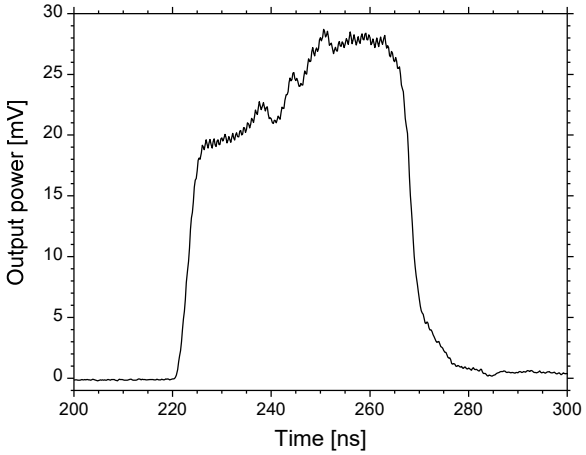

Fig. 2. THz-light power measured by the D-band diode detector.

REFERENCES:

[1] P. U. Jepsen *et al.*, Laser Photonics Rev., **5** (2011) 124.
[2] M. Gensch *et al.*, *Proc FEL2013, New York, 2013*, p. 474.
[3] N. Sei and T. Takahashi, Sci.Rep., **7** (2017) 17440.

CO12-3 High-count-rate ^{3}He position-sensitive detector readout system

S. Sato, K. Mori[1], Y. Yoshino[1], T. Seya, T. Otomo, H. Oshita, K. Okawa[2], N. Hikida[2], K. Ishizawa[2], A. Yamaguchi[3], M. Matsuura[3]

High Energy Accelerator Laboratory, KEK
[1] Institute for Integrated Radiation and Nuclear Science, Kyoto University
[2] Canon Electron Tubes & Devices Co., Ltd
[3] Clear-Pulse Co., Ltd

INTRODUCTION: Recently, the industrial use of neutrons has become widespread, and compact accelerator-driven neutron sources have been used to develop new materials. However, the development of neutron detectors that support these experimental facilities has been delayed. ^{3}He gas detectors are the most reliable neutron detectors and are typically utilized as position-sensitive detectors (PSDs) [1, 2]. However, these detectors have low count rates and low position resolutions. Therefore, joint research has begun between Canon Electron Tubes & Devices Co., Ltd. (CETD), which manufactures PSDs, and the High Energy Accelerator Research Organization (KEK), which develops readout circuits for neutron detectors.

In this research, we are developing to increase the counting rate of a ^{3}He gas position sensitive detector (PSD), and a maximum counting rate of 535 k cps has been obtained. We report the key technology of a pulse width method that has been verified of effectivity at KUR.

EXPERIMENTS: A pulse width measurement function is provided to diagnose whether a PSD can increase the count rate. This technology [3] has been developed for other detector systems. Figure 1 shows the pulse width measurement method. The pulse width is obtained by acquiring the pulse height from the pulse waveform. To determine the pulse width, the counting starts from the rising edge of the pulse and stops when it reaches half the height of the pulse. The function has been verified at the B3 beam port in KUR.

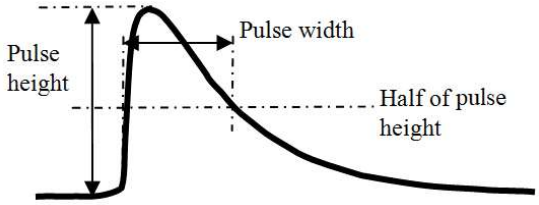

Fig. 1. Pulse-width measurement method

RESULTS: Figure 2 shows the pulse height versus width (PHW) graphs using the pulse width measurement function. The vertical axis is the pulse width (25 ns per channel), and the horizontal axis is the pulse height. Figure 2(a) shows that the entire signal gathers around 280 ns along the vertical axis, and it is a high-count-rate PSD (stopping gas: CF4, ^{3}He gas pressure: 6 atm.). Figure 2(b) shows that the low pulse height signal extends to around 700 ns, and it is a low-count-rate PSD (stopping gas: CF4, ^{3}He gas pressure: 20 atm.). The conditions are the same except that the gas pressure is different. As shown in these examples, the pulse width measurement function can identify a high-count-rate PSD.

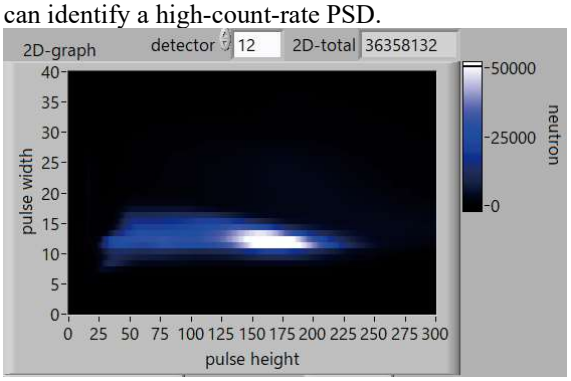

(a)

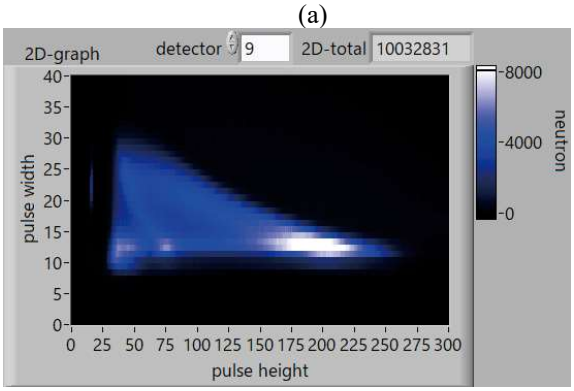

(b)

Fig. 2. PHW graphs of (a) fast PSD and (b) slow PSD

Various techniques are necessary to increase the counting rate of the ^{3}He neutron detector, and the pulse width method is an essential technique. KUR is the optimal neutron generator to verify this method.

REFERENCES:

[1] S.Sato *et al.*, EPJ Web Conf, UCANS-8, https://doi.org/10.1051/epjconf/202023105004.
[2] S. Satoh *et al.*, NIMA, **600**, 103–106 (2009), DOI 10.1016/ j.nima.2008.11.054.
[3] S. Satoh, Physica B, 551, 401–404 (2018), DOI 10.1016/j.physb.2018.03.011.

CO12-4 Neutron activation analysis of Ar in titanium metal

T. Miura, N. Yoshinaga[1], Y. Iinuma[1] and S. Sekimoto[1]

National Metrology Institute of Japan, AIST
[1]Institute for Integrated Radiation and Nuclear Sciences
Kyoto University

INTRODUCTION: National Metrology Institute of Japan (NMIJ) is responsible for developing certified reference materials and for establishing the traceability of SI (The International System of Units) on chemical metrology in Japan. To establish SI traceability, the primary method of measurements should be applied to the characterization of the certified reference materials. Recently, neutron activation analysis using comparator standard is recognized as a potential primary ratio method [1]. Despite the potential of neutron activation analysis as primary ratio method, the evaluation of the measurement uncertainty is required in any analysis. In general, there are three main components of uncertainty in neutron activation analysis, that is, sample preparation uncertainty, neutron flux homogeneity, and gamma ray measurement uncertainty. Usually, flux monitor is used to correct the neutron flux in-homogeneity. However, although the flux monitor can correct the neutron flux variation using the count rate of the known amount of the monitor nuclide, it does not reflect the neutron flux of the actual sample. The most practical method to eliminate neutron flux in-homogeneity and to improve gamma ray measurement uncertainty is an internal standard method [2, 3]. For the development of primary inorganic standard solution as national standard, the purity of starting material has to be determined. The high purity Ti metal was candidate starting material for preparation of titanium standard solution as national standard of Japan. The several trace analytical methods including neutron activation analysis, were used for purity determination of the high purity Ti metal. In this work, we presented that capability of instrumental neutron activation analysis for determination of Ar in high purity Ti metal.

EXPERIMENTS: The high purity Ti metal was purchased from Sumitomo Metal Mining Co. Ltd. The informative purity value of the Ti metal was 99.9 %. The ambient air in pre-cleaned 1 mL volume of PFA (Perfluoroalkoxy alkanes) vials were used as Ar calibration standard. The volume of PFA vials were calibrated by weighing mass of pure water prepared from Mill-Q Advance pure water system filled in each vial. The calibration of volume Mettler Toredo XP205 semi-micro balance was used for volume calibration. The calibrated PFA vials were heat sealed into Al coated polyethylene bags. One hundred mg of the Ti metal samples were used for Ar analysis. The neutron irradiations were performed by KUR (Kyoto University Research Reactor) Pn3 (thermal neutron flux: 4.7 x 10^{12} $cm^{-2}s^{-1}$) for 2 min. The γ ray measurement system consisted of an ORTEC GEM 30-76-LB-C-HJ Ge detector and a multichannel analyzer SEIKO EG & G MCA 7. Because the short-lived radioactive nuclide ^{20}F ($t_{1/2}$=11 s) was produced in PFA vial by neutron irradiation, the gamma ray measurement was started after 15 min.

RESULTS: The stable isotope ^{40}Ar produce radioactive nuclide ^{41}Ar by neutron irradiation. Usually, air contain 0.93 % of Ar. Hence, air in PFA vial can be used for calibration standard for Ar.

In this experiment, Ar in the high purity Ti metal sample could not be detected by instrumental neutron activation analysis. Therefore, the upper limit of Ar in the high purity Ti metal sample were estimated from the count rate of energy region of gamma rays emitted by ^{41}Ar induced radioactive nuclide. The estimated upper limit of Ar were $<4.0\times10^{-8}$ g/g.

Table Analytical results of Ar in high purity Ti metal

Sample	Ar g/g
Ti-a	$< 4.6\times10^{-8}$
Ti-b	$< 3.0\times10^{-8}$
Ti-c	$< 2.6\times10^{-8}$
Ti-d	$< 3.5\times10^{-8}$
Ti-e	$< 4.1\times10^{-8}$
Ti-f	$< 4.0\times10^{-8}$

REFERENCES:

[1] R.Greenberg, P. Bode, E. De Nardi Fernandes, Spectrochim. Acta B, 66 (2011) 193-241.
[2] T. Miura, K.Chiba, T. Kuroiwa, T. Narukawa, A.Hioki, H. Matsue, Talanta, 82 (2010) 1143-1148.
[3] T. Miura, R. Okumura, Y. Iinuma, S. Sekimoto, K. Takamiya, M. Ohata, A.Hioki, J. Radioanal. Nucl. Chem., 303(2105), 1417-1420.
[4] NuDat 2, National Nuclear Data Center in Brookhaven National Laboratory, https://www.nndc.bnl.gov/nudat2/index.jsp

CO12-5 A response of inner-through type ionizaiotn chamber to ^{41}Ar

A. Yunoki, H. Yashima[1], R. Okumura[1] and T. Yamada[2]

National Metrology Institute of Japan, National Institute of Industrial Science and Technology
[1]Institute for Integrated Radiation and Nuclear Science, Kyoto University
[2]Kindai University Atomic Energy Research Institute

INTRODUCTION: Equipment for continuous monitoring of radioactivity in gaseous effluents are widely used in nuclear power plants and other radiation facilities. A response of the equipment to radioactive gas is one of the most important characteristics. It is usually checked by using a sealed solid source, however, a test using radioactive gases is necessary when testing a newly developed equipment and calibrating an equipment for maintenance. In the test, the radioactive gas whose activity per unit volume is known is supplied to the equipment. Then, the response is obtained by dividing the indication of the equipment by the activity per unit volume. The activity per unit volume can be determined by using a set of proportional counters, however, this measurement is rather complexed and is not suitable for product tests. To solve this problem, the inner-through type ionization chamber, which is easier to handle, is used. The national metrology institute of Japan (NMIJ) determined the response of the inner-through type ionization chamber (Ohkura ionization chamber: type I-4096 01/06) by using a radioactive gas calibrated by the set of proportional counters. ^{85}Kr has been used for testing the monitoring equipment [1-3]. On the other hands, ^{133}Xe and ^{41}Ar are useful for obtaining an energy dependence characteristic, however, they are not commercially available. Especially, a half-life of ^{41}Ar is only 109.6 minutes, therefore, measurement needs to be finished in several hours after production. Therefore, self-production of a radioactive argon (^{41}Ar) by irradiating thermal neutrons to the stable argon (^{40}Ar) is necessary. Accordingly, we produced ^{41}Ar gas in KUR-SLY and determined the response of the inner-through type ionization chamber by using the ^{41}Ar whose activity per unit volume was determined by the set of proportional counters.

SOURCE PREPARATION: The source of ^{41}Ar was prepared by the activating stable argon (^{40}Ar) by irradiating thermal neutron. A research grade pure argon gas was poured to a small vessel of crystal glass whose volume was 10 cm^3. A pressure of the gas was 300 hPa. The vessel was sealed with petroleum jelly. Then, the vessel was placed at the bottom of the KUR-SLY operating at 1 MW for approximately 60 seconds. The nominal flux of the thermal neutron was 7.84×10^{11} [n^{-1} s^{-1} cm^{-2}]. The ^{41}Ar of 300 [kBq] was produced through ^{40}Ar (n, γ) ^{41}Ar reaction. The ^{41}Ar was then transported to Kindai University Atomic Energy Research Institute where a measurement system was temporally installed.

MEASUREMENTS: An activity of unit volume was assessed by using a set of proportional counters connected in series. Conventional pulse counting electronics were connected to the counters. The ^{41}Ar diluted by P-10 gas (nominally argon 90% and methane 10%) was flown through both the counters and the ionization chamber. The designs of the counters are the same except for their length. In order to eliminate distortion of counts near both ends of the counter, the net count rate was used which was obtained by subtracting a count rate obtained by a shorter counter from that obtained by a longer counter. The activity per unit volume [Bq cm^{-3}] was obtained by dividing the net count rate by net volume of the counter. Temperature and pressure of the gas were monitored during measurement to adjust the results to the standard condition. For impurity assessment, an energy spectrum of gamma photon from the vessel containing the ^{41}Ar was obtained by using a high-purity germanium detector.

RESULTS: Fig. 1 shows the pulse count rate as a function of a volume of proportional counter. An activity per unit volume is derived from an inclination of approximate straight line obtained by the least square method. The determined activity per unit volume was 85.3 Bq cm^{-3}. The output of inner through ionization chamber flown by the ^{41}Ar gas was 24.0 pA. Then, the response of 0.281 pA (Bq cm^{-3})$^{-1}$ was obtained. The result was adjusted to the standard condition (20℃, 101.3 kPa). As the result of gamma photon spectrometry, an amount of impurity of the sample gas of ^{41}Ar was negligible.

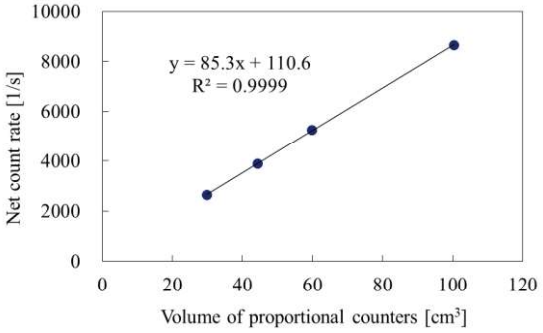

Fig. 1. Count rates as a function of a volume of proportional counters.

^{41}Ar emits gamma photon of 1293.64 keV whose emission probability is 99.157 per 100 disintegration [4]. The measurement will be improved by considering the effect of the photon to the measurement.

REFERENCES:

[1] A. Yunoki, *et. al.*, Applied Radiation and Isotopes, Vol. 68 (2010) pp.1340-1343.
[2] M Unterweger, L Johansson, L Karam, M Rodrigues and A Yunoki, Metrologia 52 (2015) S156-S164.
[3] A. Yunoki, *et. al.*, Applied Radiation and Isotopes, Vol. 134 (2018) pp.325-328.
[4] DDEP, URL: http://www.nucleide.org/DDEP_WG/DDEPdata.htm.

CO12-6 Development of neutron imager based on hole-type MPGD with glass capillary plate

F. Tokanai, T. Moriya, T. Sumiyoshi[1], H. Kondo[2], H. Sugiyama[2], M. Hayashi[2], T. Okada[2] and M. Hino[3]

Faculty of Science, Yamagata University
[1]Graduate School of Science, Tokyo Metropolitan University
[2]Electron Tube Division, Hamamatsu Photonics K. K.
[3]Institute for Integrated Radiation and Nuclear Science, Kyoto University

INTRODUCTION: Neutron imaging is useful for light elements in the sample such as hydrogen, lithium, boron, carbon, and nitrogen. Owing to their unique ability to probe inside samples, neutrons have been widely utilized for neutron radiography in various fields, including fundamental science, archaeology, and industry.

High position resolution with a moderate effective area is required in practical applications of neutron imaging. We have been developing a high-spatial-resolution neutron gas scintillation imager (n-GSI) with a capillary plate gas detector (CPGD) [1,2]. It consists of a converter layer of $^{10}B_4C$, a CPGD filled with a Ne (90%) + CF_4 (10%) gas mixture, a mirror, lens optics, an imaging intensifier unit, and a CMOS camera. A $^{10}B_4C$ converter is directly mounted on the inlet surface of the CP. Charged particles (α-rays and ^{7}Li nuclei) are generated by a nuclear reaction between incident neutrons and the ^{10}B. The charged particles ionize the gas molecules and then generate electrons in the gas. The scintillation light is emitted from the capillary holes upon gas excitation, simultaneously with electron multiplication. The scintillation light from each capillary is read out as the imaging signal through the optical mirror and lens system using an image intensified (II) CMOS camera.

Since the ^{10}B converter is directly mounted on the inlet surface of the CP, the track length of the charged particles is restricted to within the capillary. Thus, the spatial resolution of incident neutrons is expected to be close to the capillary diameter.

EXPERIMENTS: Fig. 1 shows the experimental setup. The light yield and imaging capability of the n-GSI were investigated using the cold neutron beam line CN-3 installed to the Kyoto University Reactor (KUR) [3]. The neutron wavelength giving the maximum intensity and the total flux of the CN-3 guide tube were 2 Å and 3.8 × 10^6 neutron cm^{-2} s^{-1}, respectively. The n-GSI system was placed 300 mm from the downstream exit of the neutron guide. The neutrons were irradiated into a sample.

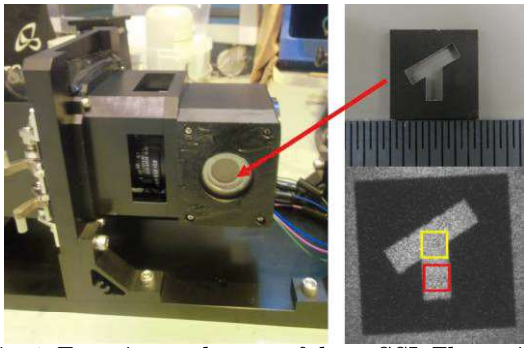

Fig. 1. Experimental setup of the n-GSI. The region of interest ROI-1 (yellow) and ROI-2 (red) are defined to investigate the light yield of the neutron transmission image.

RESULTS: The neutron transmission image of a character obtained with the n-GSI is shown in Fig. 1. The exposure time for image was 10 s. Fig. 2 shows the anode currents of the n-GSI as a function of the voltage across the CP electrode. The dependence of light yield on the voltage of ΔV is shown in Fig.3. The light yields are defined as the total counts in the ROI-1 and ROI-2, respectively. The light yield increases exponentially with the gap voltage across the CP. This result indicates that the n-GSI operates as a gas scintillation proportional counter.

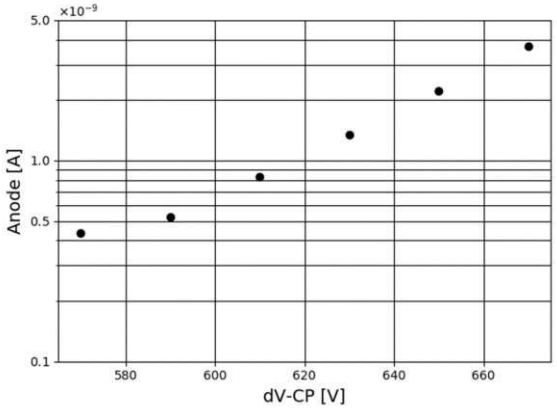

Fig. 2. n-GSI anode current as a function of the voltage across the CP electrode.

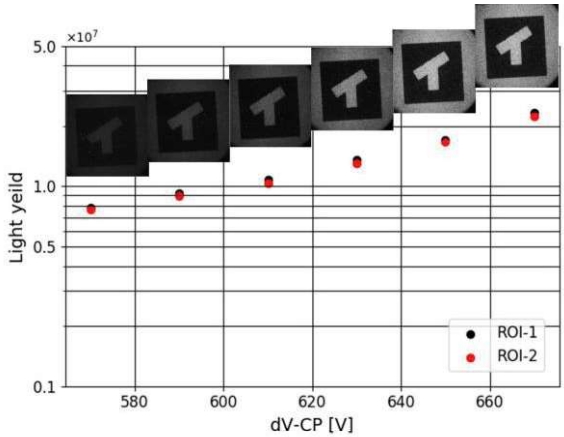

Fig. 3. Neutron transmission images and light yields as a function of the voltage across the CP electrode.

REFERENCES:
[1] H. Kondo *et al.,* Plasma Fusion Res. **13** (2018) 2406018.
[2] H. Kondo *et al.,* Nucl. Instrum. and Methods. A **958** (2020) 162804.
[3] M. Hino *et al.*, Nucl. Instrum. and Methods. A **797** (2015) 265.

CO12-7 Gamma ray measurement in the basement of the Kyoto University Research Reactor facility

K. Okada, A. Fushimi, Y. Murakami, S. Sekimoto[1], T. Ohtsuki[1], R. Okumura[1]

Center for Technology Innovation – Energy, Research and Development Group, Hitachi, Ltd.
[1] Institute for Integrated Radiation and Nuclear Science, Kyoto University

INTRODUCTION: Conventionally, fission chambers are adopted as in-core detectors for neutron flux monitoring. Part of the current value of the fission chamber during rated operation does not follow the instantaneous changes of the reactor power because decay gamma rays from reactor structure materials and delayed gamma rays from fission products have a time lag for response. However, it is difficult to separate neutron detection signals from gamma ray detection signals with a fission chamber in a high dose rate environment. Therefore, we are considering a method that monitors the neutrons only indirectly by measuring prompt gamma rays from the reactor core[1-2].

In the method, metal pieces are placed in a mixed field of neutrons and gamma rays. The prompt gamma rays emitted by the nuclear reaction between the neutrons and the metals are measured. At this time, other gamma rays around the reactor are interfering with measurements made with gamma ray spectrometers located under the reactor vessel. In this study, we used the Kyoto University Research Reactor (KUR) facility to measure the gamma_ray energy distribution under the reactor vessel to evaluate the interference gamma ray components.

EXPERIMENTS: The measurement was carried out in the heat exchanger room in the basement of the KUR facility. Two gamma ray spectrometers were used, a high purity germanium semiconductor detector (HPGe) and an $LaBr_3$(Ce) scintillation detector. Fig.1 shows the detector positions. Dose rate given in the figure was estimated in a previously done calculation[3]. The $LaBr_3$(Ce) detector was covered with a Pb shield having a collimator opened in the reactor core direction to measure the prompt gamma rays emitted from the reactor core. In order to measure the decay gamma rays around the $LaBr_3$(Ce) detector, the HPGe was covered with a shield having a collimator opened in the $LaBr_3$(Ce) direction.

The energy spectrum of gamma rays obtained with the $LaBr_3$(Ce) detector during 1 MW operation is shown in Fig.2. Total absorption peak of the 6130 keV gamma ray which was emitted by decay of N-16 in the primary cooling system pipe was seen. Both the single escape peak and double escape peak of the 6130 keV gamma ray were confirmed. In addition, total absorption peak of the 511 keV gamma ray which was emitted by decay of N-13 in the primary cooling system pipe were seen. The sum peak of the 511 keV gamma ray was confirmed. Three peaks were measured as other gamma rays. The energies of the gamma ray peaks were about 4600 keV (a), about 4100 keV (b) and about 3600 keV (c).

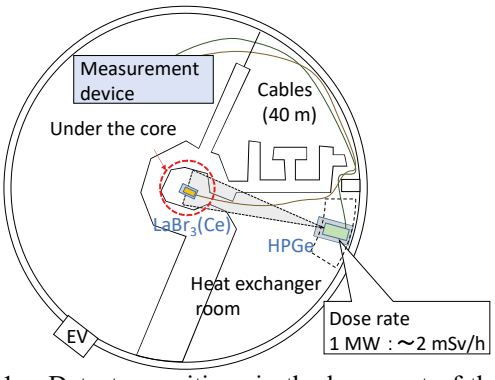

Fig. 1. Detector positions in the basement of the KUR facility.

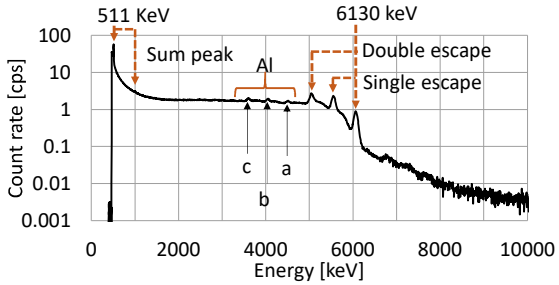

Fig. 2. Energy spectrum obtained with the $LaBr_3$(Ce) detector.

RESULTS: The energy calibration between 1022 keV (the sum peak of 511 keV) and 5108 keV (the double escape peak of 6130 keV) was difficult because there was no standard source to emit high energy gamma rays. In addition, by taking into account that the energy resolution of the $LaBr_3$(Ce) detector was too low to analyze nuclides in detail, we considered that these gamma rays were likely to be prompt gamma rays emitted from Al whose energies were 4733 keV, 4111 keV and 3465 keV[4]. Al was used as a material for a tank of the KUR. Therefore, we attribute these observed gamma rays to the Al tank.

This Al tank is equivalent to a reactor pressure vessel (RPV) or a channel box in commercial reactors. The RPV and channel box are made of stainless steel. Thus, in commercial reactors, prompt gamma rays originating from stainless steel and decay gamma rays from N-13 and N-16 interfere with measurement. In the evaluation of applicability, it is necessary to estimate the influence of the gamma rays originating from these reactor structures.

REFERENCES:

[1] K. Okada *et. al.*, J. Nucl. Sci. Technol. **57**, 514-522(2020).
[2] K. Okada *et. al.*, KURNS progress report 2018 CO12-13 (2019).
[3] K. Okada *et. al.*, KURRI progress report 2012 CO3-3 (2013).
[4] D L Anderson, *et. al.*, (ed), Kluwer Academic Publishers, Handbook of prompt gamma activation analysis with neutron beams, 190-364 (2004).

CO12-8 Neutron efficiency of a two-dimensional neutron detector with MPPC (Mpix)

H. Ohshita, H. Endo, T. Seya, Y. Yasu, M. Hino[1], T. Oda[1]

Institute of Materials Structure Science, KEK
[1]Institute of Integrated Radiation and Nuclear Science, Kyoto University

INTRODUCTION: The village of neutron resonance spin echo spectrometers (VIN ROSE) [1] is built in BL06 at the Materials and Life Science Experimental Facility (MLF). Mechanisms involving slow dynamics such as diffusion and relaxation in samples are observed by VIN ROSE. VIN ROSE consists of two spectrometers; the Neutron Resonance Spin Echo (NRSE) spectrometer and Modulated Intensity by Zero Effort (MIEZE) spectrometer [2]. The MIEZE spectrometer measures a time beat signal depending on the operation conditions of two resonance spin flippers. As it is well known, the MIEZE signal is modulated when a polarized neutron interacts with the magnetic momentum of a sample. By spring 2020, we achieved the MIEZE frequency of 800 kHz. In order to observe the slow dynamics of a sample with high accuracy, a neutron detector with a suitable time resolution under 100 ns is required. Therefore, we are developing a neutron pixel detector called Mpix. Mpix is a medium-sized neutron detector and its active area is 320 mm×320 mm. The time resolution is under 100 ns and the value is limited by the repetition of the readout electronics. A ^{6}LiF/ZnS (Ag) scintillator with 0.25 mm thickness is used as a neutron convertor. The detector also consists of 1024 Multi-Pixel Photon Counters (MPPCs) for photon counting [3]. Each MPPC is located by a 10 mm pitch, and consists of a 32×32 MPPC array. In order to measure the neutron efficiency, the neutron irradiation test was performed in CN3 [4] at the Kyoto University Reactor (KUR). This paper describes the experimental results of the neutron irradiation test.

EXPERIMENTS and RESULTS: Figure 1 shows the neutron irradiation tests to evaluate the detector performance of Mpix carried out from August 27 to August 29, 2019. The neutron efficiency of Mpix is introduced by comparing with the measurement data of a helium-3 proportional chamber (^{3}He gas filled pressure: 993 kPa). A disk chopper is worked at 30 Hz to obtain the wavelength dependence of the neutron efficiency of Mpix. Neutrons from 1.5 Å to 4 Å, pass through the disk chopper. The helium-3 proportional chamber is set downstream at the distance of 1.221 m from the disk chopper. The detector is placed in a neutron shielding case which is made from a B_4C resin. The size of the opening area of the neutron shielding case is 1 cm^2. The neutron intensity in CN3 is derived from the measurement data of the helium-3 proportional chamber with the absorption correction of the SUS detector housing. Therefore, after the estimation of the absorption correction with Geant4 [5], a toolkit to provide the simulation of the passage of particles through matter, the measurement data is converted to the neutron intensity. As a result, the expected neutron intensity in the neutron irradiation test is approximately 785.2±0.2 neutrons/s·cm^2. Furthermore, the counting rate of Mpix was measured by replacing the helium-3 proportional chamber. The neutron efficiency ε is defined as follows,

$$\varepsilon = \frac{N_{\mathrm{Mpix}}}{F_{\mathrm{n}}}$$

Where N_{Mpix} is the counting rate of Mpix and F_{n} is the expected neutron intensity in CN3. The neutron efficiency of Mpix is shown in figure 2. From the result, we found that Mpix has a thermal neutron efficiency of approximately 21%. The neutron efficiency trends to increase linearly to 2 Å, and saturates beyond that value. This is caused by the contribution of the absorption in the detector housing and the neutron detection limitation with a ^{6}LiF/ZnS (Ag) scintillator of 0.25 mm thickness. In future, we plan to further evaluate the neutron efficiency by comparing the simulation results. This work has been carried out in part under the visiting Researcher's Program of the Institute for Integrated Radiation and Nuclear Science, Kyoto University.

Fig. 1 Overview of the experimental setup.

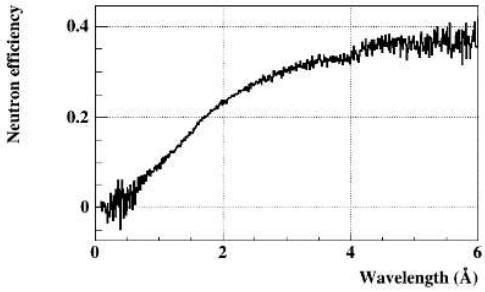

Fig. 2 Neutron efficiency of Mpix.

REFERENCES:

[1] M. Hino *et al.*, Physics Procedia, **42** (2013) 136-141.
[2] T. Oda *et al.*, J. Phys. Soc. Conf. Proc., in press.
[3] Web page of Hamamatsu Photonics K. K., https://hamamatsu.com/jp/en/index.html.
[4] M. Hino *et al.*, Annu. Rep. Res. Reactor Inst. Kyoto Univ. **27** (1994) 196-204.
[5] S. Agostinelli *et al.*, Nucl. Instr. and Meth. A **506** (2003) 250-303.

CO12-9 Research on Activation Assessment of a Reactor Structural Materials for Decommissioning (2)

M. Seki, K. Ishikawa, T. Sano[1], H. Nagata, K. Ohtsuka, T. Ohmori, H. Hanakawa, H. Ide, K. Tsuchiya, Y. Fujihara[2], J. Zhang[2] and J. Hori[2]

Department of JMTR, Japan Atomic Energy Agency
[1]Atomic Energy Research Institute, Kindai University
[2]Institute for Integrated Radiation and Nuclear Science, Kyoto University

INTRODUCTION: The radioactive waste for decommission is usually solidified by alkaline cement fillers. However, hydrogen produced by reaction of aluminum (Al) with alkaline materials may damage the waste body. Therefore, it is necessary to establish the treatment technology of radioactive Al waste for safety management of the storage facility. Last year, the irradiated Al alloy was successfully separated into relative long half-life radionuclides and Al component by our group.

In this study, the solution pH dependence of the nuclide coprecipitated with aluminum hydroxide ($Al(OH)_3$) was investigated for the purpose of recovering the Al component as $Al(OH)_3$.

EXPERIMENTS: At first, the impurities included in an Al alloy separated it by filtration within cold examination. These solutions were analyzed of elementals by ICP-AES.

Secondly, the Al samples were irradiated in Pn-2 of KUR pneumatic transportation facility and cooled for 4 days. The irradiation condition and chemical composition of the sample are listed in Table 1 and Table 2, respectively. After the irradiation, sodium aluminate ($Na[Al(OH)_4]$) was produced by dissolving the samples in NaOH solution with pH of 5 - 11. The insoluble impurities included in the sample were separated by filtration. This solution was neutralized by hydrochloric acid (HCl) to precipitate as $Al(OH)_3$. The radioactivity of the impurities and $Al(OH)_3$ were measured by a germanium semiconductor detector so as to investigate chemical behavior of the radionuclides.

Table 1 Irradiation conditions of sample in Pn-2.

Items	Values
Thermal power	5 MW
Thermal neutron flux	2.8×10^{17} $m^{-2}s^{-1}$
Epithermal neutron flux	1.1×10^{16} $m^{-2}s^{-1}$
Fast neutron flux	6.0×10^{16} $m^{-2}s^{-1}$
Irradiation time	20 min.
Cooling time	4 days
Sample	0.25 g

Table 2 Chemical Compositions of sample.

	Si	Fe	Cu	Mn	Mg	Cr	Zn	Ti
rate [%]	0.61	0.42	0.28	0.02	0.99	0.24	0.01	0.04

RESULTS: Table 3 shows the results of Al recovery by ICP-AES. In pH = 7 and 9, the Al concentration of this solution was less than detection lower limit level.

In pH = 5 and 11, it was revealed that Al could be collected 85% or more as $Al(OH)_3$. In addition, the NaCl was produced with $Al(OH)_3$ and included by $Al(OH)_3$.

Secondly, a hot examination was conducted similarly. $Al(OH)_3$ was measured radioactivity by a germanium semiconductor detector after it was filtered and enough to be wash with ion exchanged water. As a result, Cr-51 and Na-24 coprecipitated with $Al(OH)_3$ were obtained. Cr-51 was produced by a reaction of (n,γ) which was impurities element of A6061. Na-24 was produced by Al-27 (n, α) Na-24.

Cr-51was equal values under conditions of all. In Na-24, pH = 5 is maximum, because there was much produced NaCl and quantity of Na-24 Cl was included in $Al(OH)_3$ more than other conditions.

Table 3 The results of Al recovery by ICP-AES.

pH	① Meltability [mg]	② Quantity of a filtrate [mg]	①-② [mg]	③ Recovery [%]
5	100.0	0.40	99.60	99.6
7	100.0	<0.05*	99.95	100.0
9	100.0	<0.05*	99.95	100.0
11	100.0	13.70	86.30	86.3

* The detection lower limit value

Table 4 The results of radioactivity measurement with the germanium semiconductor detector [Bq / Al-1g].

pH	5	7	9	11
Cr-51	1.67×10^{1}	1.82×10^{1}	2.36×10^{1}	2.20×10^{1}
Na-24	2.11×10^{5}	2.79×10^{4}	1.85×10^{4}	3.06×10^{4}

CONCLUSION: The radionuclide which coprecipitated with $Al(OH)_3$ were Cr-51 and Na-24Cl was included in the NaCl which was produced at the same time when $Al(OH)_3$was produced.

In future, an experiment scale would be scale up the model and A more realistic processing condition is demanded.

REFERENCES:

[1] Taichi Sato, Journal of the Mineralogical Society of Japan, 19(1), 1989, pp.21-41.
[2] Gitzen, W.H. (ed.), Alumina as a ceramic material., American Ceramic Society, 1970.
[3] M. Seki, *et al.,* KURNS Progress Report, p.257, 2018.

CO12-10 **Beam Test of a micro-cell MWPC for a muon-electron conversion search experiment, DeeMe**

M. Aoki, N. Abe[1], Y. Higashino, H. Ikeuchi[2], K. Komukai[2], D. Nagao, H. Natori[3], Y. Seiya[2], T. Takahashi[1], T. Takahashi[2], N. Teshima[2], K. Yamamoto[2] and S. Yamashina

School of Science, Osaka University
[1]Institute for Integrated Radiation and Nuclear Science, Kyoto University
[2]Faculty of Science, Osaka City University
[3]Institute of Materials Structure Science, KEK

INTRODUCTION: Charged-lepton flavor violation (CLFV) process such as $\mu \to e\gamma$, μ-e conversion, τ-CLFV decays are heavily suppressed in the standard model of particle physics (SM). However, in the most of the models beyond SM, it is considered to be occurred with a strength that can be reached in the coming experiments. DeeMe is one of experiments that aims to search for μ-e conversion in nuclear field [1] at a level of 10^{-13} of the branching ratio in the single event sensitivity. It uses high-power high-purity pulsed proton beam from J-PARC RCS. The detector of DeeMe should be operational after $\mathcal{O}(\mu s)$ from a burst of particles (100 GHz/mm^2) produced by the proton pulse. In order to solve the problem, a multi wire proportional chamber (MWPC) with high-volt-age switching technique was successfully developed [2]. It is very important to improve the total performance of the MWPC before the start of the physics data taking at J-PARC MLF in order for better physics sensitivity.

EXPERIMENTS: Two experiments were performed in this fiscal year. In the 1st experiment, three MWPCs were sequentially placed so that the beam electrons from the KURNS electron LINAC hit through all three of them. The MWPC performance with three different gas mixtures were tested, where gas mixtures of Ar : i-C_4H_{10} : R-134a were 74:20:6, 70:20:10 and 65:20:15. At first, the burst electrons (10^7 electrons/200-ns/360-mm^2) with energy being 16 MeV were injected to the MWPCs at the timing when they were in the off-state. The MWPCs were turned to on-state right after each burst, and the amount of delayed false pulses induced on the read-out electrode strips were measured by using Fast-FADC system [3]. Less delayed false pulses were seen as the mixture of R-134a increases. Next, the burst electrons were turned off and the MWPC efficiencies were measured with low rate DC electrons at 16 MeV energy from the LINAC. The time averaged efficiencies are (94.2 $\pm$ 0.6)%, (87.7 $\pm$ 0.4)% and (73.3$\pm$0.5)% for 6%, 10% and 15% of R-134a fractions, respectively. Finally, the electron energy was increased to 30 MeV, and the position resolution of MWPC was measured. The quick off-line analysis shows that the position resolution is better than 1 mm (rms) including the multiple scattering effect, which is sufficient for the physics data taking in μ-e conversion search.

In the 2nd measurement, a prototype MWPC was used with methylal-mixed gas instead of R-134a mixed gas since the goodness of the performance of the ion absorption by methylal has been well known, and expected to outperform R-134a. The gas system was modified so that liquid methylal shall be mixed to the Ar and i-C_4H_{10} mixed gas with a precisely controlled mixture fraction. Figure 1 shows a correlation between delayed false pulse rate and a pulse height of real hit that produced by an electron hitting through the MWPC. The unit of the delayed false pulse rate is arbitrary. The red-filled circle labeled as 1510 V corresponds to the same configuration of the gas we obtained 73.3% of efficiency in the 1st measurement. The blue-triangle labeled as 1460 V provides two-times higher gas gain with two- times smaller delayed false pulse rate.

RESULTS: The positional resolution of MWPC measured with higher energy than that we used in the previous study shows better value, and it is sufficient for the purpose of DeeMe. A beam test with a prototype MWPC revealed that the delayed false pulse can be suppressed by using methylal-mixed Ar and i-C4H10 gas while maintaining good gas gain. The final performance should be checked by using a production-version of MWPC in 2020.

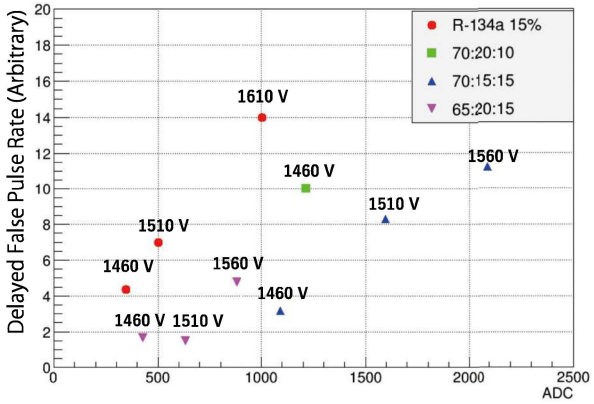

Fig. 1 Correlation between the delayed false pulse rate and signal gain. See text for more details.

REFERENCES:

[1] N. Teshima on behalf of the DeeMe Collaboration, "DeeMe experiment to search for muon to electron conversion at J-PARC MLF", in proceedings of NUFACT conference PoS (NuFact2017) 109 (2018).
[2] H. Natori, *et al.*, "A fast high-voltage switching multi-wire proportional chamber", Prog. Theor. Exp. Phys. 2017(2) 023C01 (2017).
[3] N.M. Truong, *et al.*, "Real-Time Lossless Compression of Waveforms Using an FPGA", IEEE Trans. Nucl. Sci. 65 2650 (2018).

CO12-11 An attempt to produce carrier free tracer through photonuclear reaction and hot atom effect

T. Kubota, K. Takamiya, S. Fukutani and Y. Shibahara

Institute for Integrated Radiation and Nuclear Science, Kyoto University

INTRODUCTION: Photonuclear reactions can produce radioisotopes which are hardly produced through neutron irradiation. The production reaction and its rate depend on the energy of photons. Photons are usually generated through the irradiation of high-energy electrons to heavy metal. The KURNS-LINAC can accelerate electrons up to 46 Mev, hence in this limitation (γ, n) reaction is dominant. The effective cross-section of this reaction is roughly 100 times as large as other reactions, such as (γ, 2n), (γ, p), and (γ, np) reactions [1-2]. It is desirable that the (γ, n) reaction is used to produce radioisotopes. In the case that radio isotopes are used for biological experiments as tracer, carrier free ones, whose specific activity and purity is high, are required in order to avoid chemical toxicity. However, carrier free isotopes cannot be produced through (γ, n) reactions because products are basically the same element as target. In order to solve this difficulty, the production of carrier free isotopes was attempted by hot atom effect. As an example, Shibata et al. reported that a mixture of UO_2 and NaCl was irradiated with neutrons and recoil fission products were trapped inside soluble NaCl and were separated from insoluble UO_2 by adding water [3]. In this research radioisotopes were produced through photon irradiation to a mixture of oxides and salts.

EXPERIMENTS: Fe_3O_4 and MoO_3 were used as oxide and NaCl and KCl as salt, and the composition of a mixture is listed in Table 1. Each mixture was homogenized by grinding in a mortar and pestle and then was encapsulated in a quartz test tube under vacuum. The quartz test tube was irradiated with photons generated by the bombardment of 30 MeV electrons to platinum sheet of 2 mm thick at the KURNS-LINAC. The platinum sheet and quartz test tube were cooled by cooling water and blowing air, respectively. The irradiation time is listed in Table 1. After the decay of short half-life nuclides in irradiated materials, they were transported to the Tracer laboratory and subject to further treatment. The mixture was added with water to suspension solution, and this solution was transferred from the quartz tube to a polyethylene centrifugation tube. The quartz test tube was washed twice with water, and the washing solution was combined with the suspension solution. The centrifugation tubes were added with water to dissolve salt completely, shaken, and centrifuged to precipitate oxides. The aqueous phase was separated from the residue phase. The radioactivity of both phases was determined by γ-spectrometry and yielded the fraction of radionuclide produced from oxide phase to salt phase through a hot atom effect.

Table 1 Irradiation condition

Sample ID	#1	#2*	#3
Fe_3O_4	0.90 g	2.40 g	
MoO_3			0.14 g
NaCl	2.05 g		
KCl		27.31 g	0.91 g
Irradiation time	12 hr	6 hr	1 hr

* An aliquot of the mixture was used for irradiation.

RESULTS: Irradiation of chloride provided Cl-34, which was dominant radioactivity immediately after irradiation and was, however, trivial matter due to its short half-life. On the other hand, irradiation of sodium provided long half-life Na-22, which was required to be removed, if necessary. The use of KCl was therefore desirable as binding salt. Table 2 shows the transfer fraction of Fe-52 and Mo-99 from the oxide phase to the salt phase, as carrier free tracer of iron and molybdenum, respectively. The value of Fe-52 was calculated from the radioactivity of Mn-52, and was lower than the detection limit, showing that no activated iron element was liberated from iron oxide crystal. The value of Mo-99 was 3%; however, during the water treatment the solution turned to blue purple, showing the dissolution of matrix MoO_3 and no longer carrier free solution. In conclusion the production of carrier free tracer through photonuclear reaction and hot atom effect requires alternative methods.

Table 2 Transfer fraction by hot atom effect

Sample ID	#1	#2	#3
Mixture	Fe_3O_4 NaCl	Fe_3O_4 KCl	MoO_3 KCl
Tracer	Fe-52/Mn-52	Fe-52/Mn-52	Mo-99
Transfer fraction	~0 %	~0 %	3 %

REFERENCES:

[1] T. Kubota *et al.*, KURRI Progress Report 2014 (2015).
[2] T. Kubota *et al.*, KURRI Progress Report 2017 (2018) 209.
[3] S. Shibata *et al.*, Applied Radiation and Isotopes **60** (2004) 625–628.

CO12-12 Study of Isotope Separation via Chemical Exchange Reaction

R. Hazama, T. Yoshimoto, A. Rittirong, Y. Sakuma[1], T. Fujii[2], T. Fukutani[3], Y. Shibahara[3]

Graduate School of Human Environment, Osaka Sangyo University
[1]Laboratory for Advanced Nuclear Energy, Tokyo Institute of Technology,
[2]Graduate School of Engineering, Osaka University
[3]Institute for Integrated Radiation and Nuclear Science, Kyoto University

INTRODUCTION: Chemical isotope separation for calcium has been studied in liquid-liquid extraction (LLE) with an appropriate crown-ether (CE) by utilizing a conventional batch (macroscopic) method [1] and a cutting edge micro-reactor/chip method [2]. Based on the measured reaction time between organic and aqueous solution seems fast (less than a minute) (Fig.1), a new test tube method has been pursued and its Ca mass balance between two phases was confirmed (Fig. 2) as with the case of batch and micro-reactor/chip methods.

EXPERIMENTS: Isotopic enrichment occurs according to the following chemical exchange reaction:

$$^{40}Ca^{2+}_{(aq)} + {}^{48}CaL^{2+}_{(org)} \rightarrow {}^{48}Ca^{2+}_{(aq)} + {}^{40}CaL^{2+}_{(org)} \quad (1)$$

where L represents macrocyclic polyether(18-crown-6). An aqueous solution (3M $CaCl_2$) and organic solution (0.07M DC18C6 in chloroform) were stirred by a magnetic stirrer with changing a mixing time from 0 sec (no-mixing) to 60 min at room temperature and separated with a constant standing time of 30 min. The Ca concentration for both phases was measured by AAS in Fig. 1.

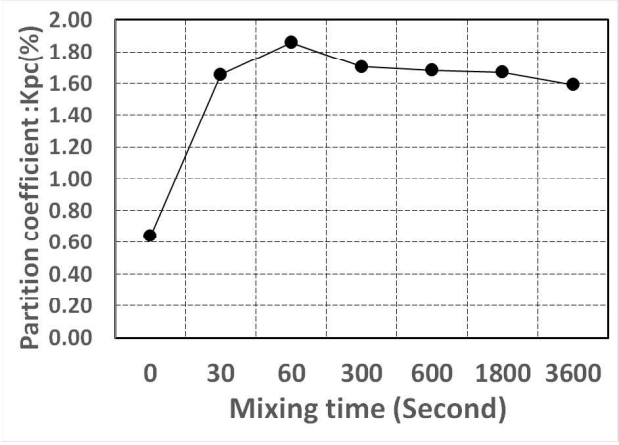

Fig 1. The partition coefficient (Kpc) (= (Ca concentration in organic phase) / (Ca concentration in aqueous phase) was measured by changing the mixing time of 0 (no-mixing), 30 sec and 1, 5, 10, 30, 60 min: Preliminary.

A new test tube method was studied with the same two phases stirred by hand (only a second), separated by a centrifuge with 3 min, and iterated for fifteen times. The Ca concentration of both phases was measured by AAS and its Ca transfer between the two phases and no loss to the other medium was confirmed in Fig.2.

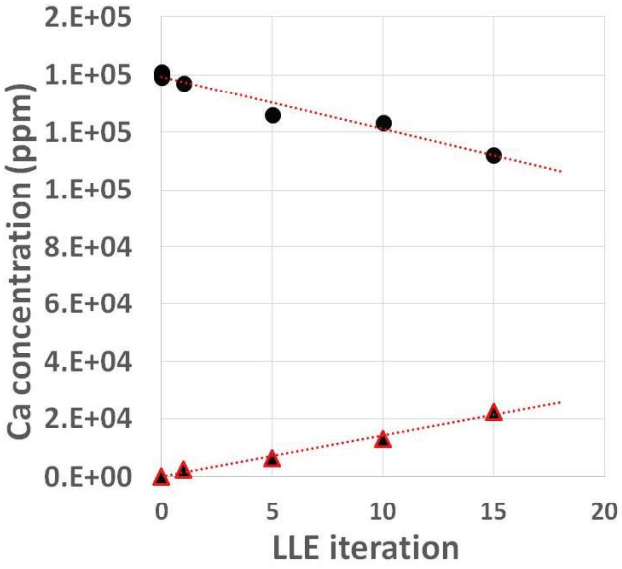

Fig 2. Ca concentration in aqueous phase (circle) and organic phase (triangle) for the process of LLE. Iteration is 15 times, zero is feed solution for $CaCl_2$ aqueous and crown-ether organic ($CHCl_3$) phase: Preliminary.

RESULTS: It is noted that one process of this mixing/separation is only a few minutes and it takes less than an hour for the total of fifteen times multistage process. More than 3000 multistage enrichment process for ten times enrichment of Ca natural abundance can be achieved for a week and the scale-up for the mass production with an order of ton size is also promising due to this simple and easy handling procedure by utilizing the lab shaker and centrifugal separator in Fig. 3

Fig 3. An example of lab shaker (Right) and centrifugal separator (Left).

REFERENCES:

[1]R. Hazama *et al*., KURRI Progress Report 2017, 104.
[2]R. Hazama *et al*., KURRI Progress Report 2018, 252.

CO12-13 Radius of Gyration of Polymer for Viscosity Index Improver at Various Temperatures Evaluated by Small-Angle X-Ray Scattering

T. Hirayama, R. Takahashi[1], Y. Takashima[2], K. Tamura[2], N. Sato[3], M. Sugiyama[3]

Dept. of Mechanical Eng. and Science, Graduate School of Kyoto University
[1]Dept. of Mechanical Eng., Graduate School of Doshisha University
[2] Idemitsu Kosan Co., Ltd.
[3]Institute for Integrated Radiation and Nuclear Science, Kyoto University
[4]Japan Atomic Energy Agency

INTRODUCTION: Lubricating oils are necessary for friction reduction and high wear durability of sliding surfaces in machine components, and the development of the best oils is strongly required from industry. Viscosity index improver (VII) is a kind of additives for relieving the reduction of viscosity of lubricating oil due to temperature rise. Classical textbooks say that the VII molecules work with changing their equivalent radius in base oil in accordance with oil temperature. However, there are only few papers investigating the equivalent radius of VII molecules by small-angle X-ray scattering (SAXS) and/or small-angle neutron scattering (SANS)[1], and there is still room for discussion of the behavior and working mechanism of VII molecules in oil. This study tried to investigate the radius of gyration of several kinds of VII polymers in base oil at various temperatures by SAXS, and the behavior of polymers was investigated and discussed.

EXPERIMENT: To investigate the radius of gyration of VII polymer, we used a SAXS instrument (NANOPIX, Rigaku) with a Cu-target X-ray source emitting X-ray with a wavelength of 1.54 Å, a characteristic line of Cu-Kα. The 1.2 mm-thick aluminum cell having optical windows made of 20-μm thermally-resistant engineering plastic film (Superio-UT, Mitsubishi chemical) was used for the measurement. The cell temperature increased to be 25, 40, 60, 80 and 100°C in turn, and the last measurement was carried out at 25°C again after cooling for checking if the VII molecule degenerated or not by heat. Poly(methyl acrylate) (PMA) type VII, as shown in Fig. 1, was prepared as a typical one used in engine oil in the study. Squalane was used as a model base oil, and the concentrations of PMA into squalane were 0.5, 1.0 and 2.0 mass%.

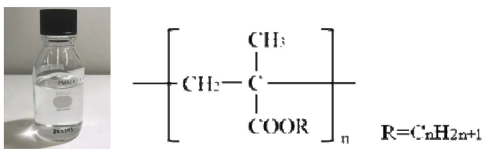

Fig. 1. Chemical structure of PMA type VII.

RESULTS AND DISCUSSION: The SAXS intensity profiles versus scattering vector q from squalane with 0.5 and 2.0 mass%-PMA type VII at each temperature were shown in Fig. 2, for example. The profiles were obtained by subtracting the intensity profiles from pure squalane at each temperature previously measured with the same liquid cell. The radius of gyration R_g estimated from the Guinier plot is shown in Fig. 3. We can see that the intensity profiles had little change even if the temperature changed, but the estimated R_g was gradually increased in accordance with the temperature rise even though the change of R_g was not so large. The trend of R_g change was similar with the R_g estimated by SANS and R_η estimated from the actual viscosity change. From the whole measurement, we succeeded to estimate the behaviour of PMA type VII against the temperature rise as shown in Fig. 4.

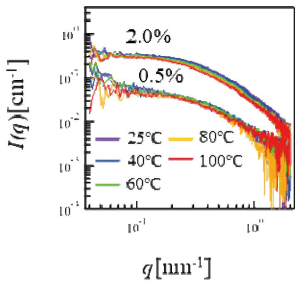

Fig. 2. SAXS profiles from squalane with 0.5 and 2.0 mass%- PMA type VII at various temperatures.

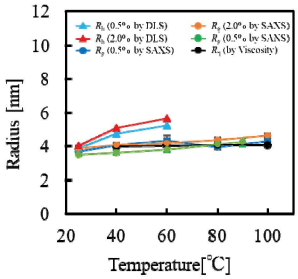

Fig. 3. Estimated Rg from Guinier plot of squalane with PMA type VII with various concentrations.

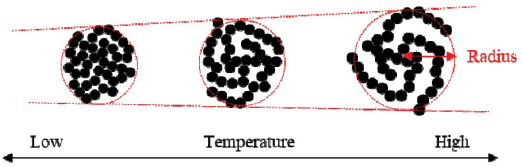

Fig. 4. Structure of PMA type VII with temperature change.

REFERENCES:

[1] M. J. Covitch, K. J. Trickett, How Polymers Behave as Viscosity Index Improvers in Lubricating Oils, Adv. Chem. Eng. Sci., 5 (2015) 134.

CO12-14 Friction Reduction by the Combination Use of MoDTC and Organic Friction Modifier

T. Hirayama, N. Yamashita[1], M. Hino[2]

Dept. of Mechanical Eng. and Science, Graduate School of Kyoto University
[1]Dept. of Mechanical Eng. and Science, Graduate School of Kyoto University
[2]Institute for Integrated Radiation and Nuclear Science, Kyoto University

INTRODUCTION: Engine oil is a blend of base oil such as mineral oil and synthetic oil with additives, and it contributes to saving fuel by reducing the friction loss of the engine. Therefore, among various additives, those having a friction reducing effect under boundary lubricated conditions are blended in the engine oil, of which molybdenum dithiocarbamate (MoDTC) is particularly effective. MoDTC is known to produce a boundary lubrication layer containing molybdenum disulfide (MoS_2), which is effective for reducing friction. In addition, it is recently expected that a system using a combination organic friction modifier (OFM) that has no phosphorus in its molecule and MoDTC will alleviate environmental problems and obtain a sufficient friction reducing effect. The lubrication properties under boundary lubricated conditions are greatly influenced by the interfacial structure of the boundary lubrication layer formed by additives. Therefore, the interfacial structure formed by the combination use of MoDTC and OFM and its nanotribological properties were investigated in this study.

EXPERIMENTS: In this study, the oil in which MoDTC (0.3 mass%) and OFM is added to the base oil was used as the lubricating oil model. Hexadecane and palmitic acid (0.1 mass%) were used as models for the base oil and OFM. For neutron reflectometry (NR), deuterated palmitic acid, was used for the purpose of facilitating the analysis since a clear difference occurs in the reflectivity profile between hydrogen and deuterium.

We used the time-of-flight (TOF) type neutron reflectometer SOFIA installed at the J-PARC in Tokai, Ibaraki. In order to grasp the film thickness and density of the boundary lubrication layer formed on the Cu surface under each system added alone or in combination, experiments were conducted to obtain the reflectivity profile under each case.

RESULTS: First, we conducted the NR experiment to investigate the boundary layer structure formed by *d*-palmitic acid. When *d*-palmitic acid was added, the fringe interval became short; as a result of the analysis, it was found that an adsorption layer having a thickness of about 2.1 nm was formed on the copper surface immediately after the addition of *d*-palmitic acid. The SLD value of *d*-palmitic acid at the bulk state was 6.7×10^{-6} Å^{-2}, whereas the analysis value was 2.1×10^{-6} Å^{-2}. From this, the density of the adsorption layer was approximately 30% with respect to the bulk density. From 0h to 2h, the fringe interval did not change; it indicated that the film thickness and the density of the adsorption layer by *d*-palmitic acid barely change with time.

For the combined system being used, measurements were carried out under the three cases described below. [Case 1]: Measurement was carried out for four hours after placing hexadecane+*d*-palmitic acid (0.1 mass%) + MoDTC (0.3 mass%) into the sample holder. [Case 2]: Measurement was carried out for two hours after hexadecane+*d*-palmitic acid (0.1 mass%) was placed in the sample holder. After the measurement, the sample holder was rinsed with hexadecane, and hexadecane+ MoDTC (0.3 mass%) was added, and then the measurement was carried out for four hours. [Case 3]: Measurement was carried out for four hours after hexadecane+MoDTC (0.3 mass%) was placed in the sample holder. After the measurement, the sample holder was rinsed with hexadecane, and hexadecane+*d*-palmitic acid (0.1 mass%) was added, and then the measurement was carried out for two hours.

As a result of analysis of [Case 1], it was found that an adsorption layer with a thickness of about 2 nm and a density of approximately 30% with respect to the bulk density was formed immediately after *d*-palmitic acid was added. Although the film thickness did not change with time, the density increased to about 60% in four hours. When MoDTC is added first, film thickness and density cannot be detected since MoDTC was not deuterated. However, from the NR experiment of [Case 3], it can be seen that immediately after the addition of *d*-palmitic acid, an adsorption layer having the 2-nm film thickness and the approximately 30% density with respect to the bulk density is formed. While no change in film thickness with time was observed, the density increased from about 30% to about 45% in 2 hours. This result is shows the same tendency with as [Case 1]. In addition, it is interesting to note that the nanotribological property measured by SiO_2 colloidal probe was better when we used MoDTC and palmitic acid in combination than that when we used only MoDTC or palmitic acid each. It indicated that the combination use of MoDTC and OFM is effective for friction reduction by forming thicker boundary lubrication layer.

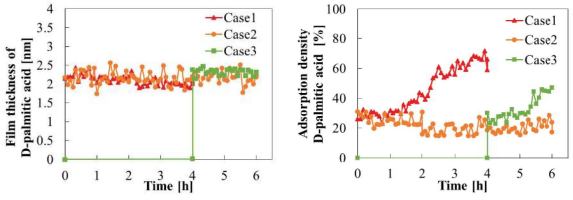

Fig. 1. Estimated film thickness and density of palmitic acid by neutron reflectometry for the three cases.

CO12-15 Multi-element neutron activation analysis of selected Japanese food samples by neutron activation analysis

M. Fukushima, T. Maeda and Y. Iinuma[1]

Faculty of Sciences and Engineering, Ishinomaki Senshu University
[1]Institute for Integrated Radiation and Nuclear Science, Kyoto University

INTRODUCTION: It is important to obtain multi element levels in food samples for nutritional purposes. For the analysis of multi elements in food samples, atomic absorption spectrometry (AAS) and induced cou-pled plasma spectrometry (ICP-AES) are widely used after pre-treatment of acid extraction or acid digestion. Though complete acid digestion is needed for obtaining total levels of elements in food samples, it is not easy by the presence of high concentrations of lipids, polysaccha-rides, *etc*. preventing acid digestion. For eliminating this problem, neutron activation analysis was used for multi elements analysis of Japanese food samples. Bioaccessi-ble trace element levels in soft tissues of oysters were also estimated by using an AOAC method.

EXPERIMENTAL: Vegetables, fish, mushroom, seaweeds, and wild plants were collected from Ishinomaki farmers and fish markets mainly in 2017-2019. Samples were washed with tap water, separated edible parts, freeze dried, and pulverized for dried powder samples. NAA was done by three different conditions according to nuclides for the interest. 1) One portion of samples was irradiated for 1-1.5 min in TcPn site. After 3 minutes decay, gamma spectrum was measured for 10 minutes by Ge detector with CSS. Levels of Br, Ca, Cl, I, K, Mg, Mn, Na, and V were analyzed using ^{80}Br, ^{49}Ca, ^{38}Cl, ^{128}I, ^{42}K, ^{27}Mg, ^{56}Mn, ^{24}Na, and ^{52}V. 2) Another portion of samples was irradiated for 20 minutes, and gamma spec-trum was measured for 20 minutes after 2-3 days decay for analyzing As using ^{76}As. 3) Another portion of samples was irradiated for 1 hour, and gamma spectrum was measured for 20 minutes after 1month decay for analyzing Ag, Co, Cr, Cs, Fe, Rb, Sc, Se, and Zn using ^{76}As.1 h in the Kyoto University Reactor, Japan. Gamma-ray spectra of the irradiated samples were recorded after one-month decay for 20-30 min using a Ge detector system. Levels of Ag, Co, Cr, Cs, Fe, Rb, Sc, Se, and Zn were obtained using ^{110m}Ag, ^{60}Co, ^{51}Cr, ^{134}Cs, ^{59}Fe, ^{86}Rb, ^{46}Sc, ^{75}Se, and ^{65}Zn, respectively. NAA method used was validated using NIST SRM 1570a Spinach Leaves, NIST SRM 1566b Oyster Tissue, NIST SRM 1575 Pine Needles, NIST SRM 1573a Tomato Leaves, and NIST SRM 1548a Typical Diet.

Bioaccessible trace element levels in food samples were estimated for several fish samples by using an AOAC method. Briefly, about 1 g of dried oyster soft tissue powders was incubated with α-amylase, protease, and amyloglucosidase one after another. Water soluble dietary fiber was filtered from the undigested residue after adding ethanol, and both fractions were analyzed by INAA.

RESULTS: Ag was found only in dried sakuraebi and ami. I and V were found only in seaweeds. Several data obtained for fish samples are shown in Table 1.

Table 1. Levels of elements in fish muscle
(unit: mg/kg, dry weight)

Fish sample	Cs	Fe	Se	Zn
Tuna red muscle	0.31	35.8	2.75	16.8
Tuna medium fatty muscle	0.20	22.4	2.11	13.5
Skipjack tuna without dark muscle	0.15	38.1	2.17	21.8
Skipjack tuna_ dark muscle	0.20	313.6	12.38	25.9
Salmon	0.45	11.4	2.32	11.7

From the results in Table 1, differences of Fe and Se levels between skipjack tuna muscle dark muscle and without dark muscle were remarkable.

Bioaccessible levels of Se in fish sample were obtained, and the ratios of bioaccessible Se to total Se were; 0.45, 0.39, 0.51, 0.56, and 0.46 for tuna red muscle, tuna medium fatty muscle, skipjack tuna without dark muscle, skipjack dark muscle, and salmon, respectively. It may be said that about half of total Se is bioaccessible level.

Wild plants analyzed were; shidoke, Ostrich Fern, alpine leek, fiveleaf aralia, Aralia sprout, udo, butterbur, bracken, mizu, urui, bonna, Japanese parsley, and bamboo shoots from 4 different collection areas. Several levels of elements in wild plants were interesting when compared to ones of vegetables. For example, Mn levels in 13 species, except shidoke, fiveleaf aralia, and Japanese parsley, were high, though Mn levels in 32 vegetables were under the detection limit. Mn levels were 244 - 3620 mg/kg, DW in brackens, 2910 mg/kg, DW in bonnna, 1540 mg/kg, DW in udo. Also, several elemental levels showed difference between collection area, and showed in Fig.1. Fig. 1 shows difference between three shidoke collected from Yamagata Prefecture, Kahoku (Ishinomaki, Miyagi), and Kamaishi (Iwate Prefecture).

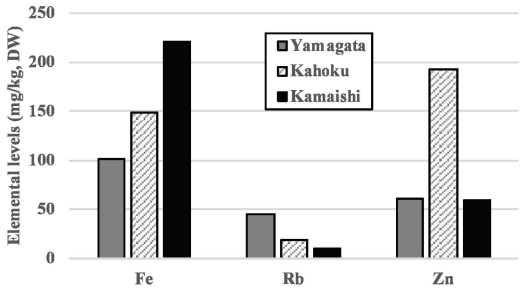

Fig.1. Elemental levels of shidokes collected from three different areas.

31123

M.A. Soliman, K. Takamiya, T. Kubota, R. Okumura and T. Ohtsuki

Institute for Integrated Radiation and Nuclear Science, Kyoto University

INTRODUCTION: Flowing sample neutron activation analysis (FSNAA) is a subclass of NAA, which has been developed for analysis of water/liquid samples [1]. It involves continuous pumping a large volume of the sample, in a tube, between the irradiation site and the γ-ray detector [1]. Analysis of large volume of a sample improves the detection limits, while continues pumping allows better measurement of short-lived radionuclides. The set-up was previously investigated for analysis of synthetic and real samples using ^{252}Cf as a neutron source [1, 2]. The purpose of the present work is to install FSNAA at the slant irradiation tube of KUR to take the benefit of its high flux.

EXPERIMENTS: Irradiation durability test was performing to select a suitable tubing material. Samples of polyethylene, TYGON, and Ethylene tetrafluoroethylene tubes were irradiated for different periods and then a simple bending test was performed [3].
The FSNAA set-up was constructed (Figure 1) using the selected tube. The tube was rolled around the HPGe detector to increase the counting time. The general procedures including: placing the sample in a sample tank, pumping it to the irradiation site, and then record a gamma-ray spectrum with HPGe. Finally the irradiated sample was stored in a storage tank. A run with de-ionized water was carried out for leakage test and to check the performance of the set-up components as well as for background measurements. FSNAA was tested for analysis of tap (from KURNS) and Kashii River waters samples based on relative method using multi-elements reference standard solution. The analyzed sample volume was ~1 l and the flow-rate was 30 ml/min.

RESULTS: However, irradiation durability test showed that all tested tubes have acceptable radiation resistance, TYGON was used for constructing the system due to its low chorine content and excellent bending flexibility.
Table 1 shows the analysis results of tap water and river water samples. Nine elements were detected and quantified, while Cl, Br, I, and ^{18}O were detected but not quantified due to the lack of reference standard. Levels of the quantified elements in the tap water are below the WHO guidelines [4]. The detection limits obtained from this preliminary FSNAA study are satisfied in comparison to conventional NAA and other techniques. Under the current experimental conditions, the decay time (the travelling time between the irradiation site and HPGe) was ~ 3.5 min. This relatively long decay time hinders the analysis of several elements (those with shorter half-lives isotopes ex: ^{20}F, ^{46m}Sc, ^{77m}Se, ^{107m}Pb,…).

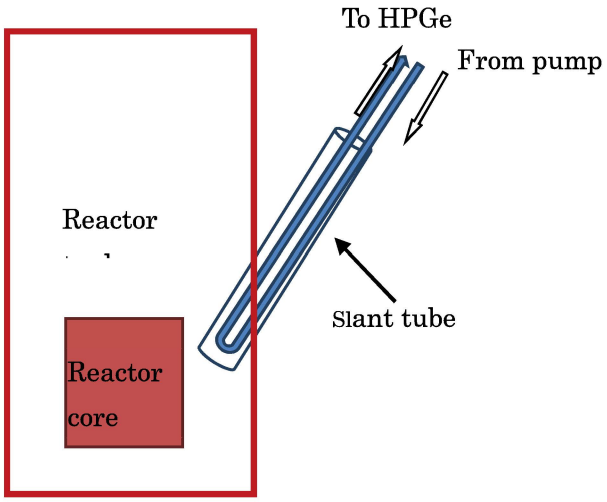

Fig 1. FSNAA setup installed in slant tube

Also, it adversely affects the detection limits of ^{28}Al, ^{52}V, and ^{66}Cu due to the decay of major fraction of their radioactivities before reaching the HPGe.
As a future plan, use of powerful pump will reduce the decay times; and hence it is expected to increase the number of measured elements and improves the detection limits for some elements like Al, V, and Cu. The capability of FSNAA to measuring ^{18}O reveals its potential for determining past climate temperatures using, for example, water samples collected from ice cores.

Table 1. Analysis results of tap and river water samples

	Tap water		River water	
Element	µg/l ± %	DL	µg/l	DL
O (^{19}O)	D		D	
Na	9700 ± 2	110	8800 ± 2	105
Mg	1300 ± 5	135	3720 ± 3	200
Al	25.5 ± 6	2.2	240 ± 1.3	2.0
S	8000 ± 25	7400	10500 ± 20	6600
Cl	D		D	
K	1350 ± 23	980	1350 ± 25	1180
Ca	10100 ± 4	280	15900 ± 2.5	240
V	0.40 ± 14	0.14	0.37 ± 15	0.15
Mn	1.7 ± 30	1.5	132 ± 2	1.9
Cu	28.0 ± 35	25	ND	
Br	D		D	
I	D		D	

D: detected only, DN: not detected

REFERENCES:

[1] M. Soliman *et al.*, J. Radioanal. Nucl. Chem., **295** (2013) 245-254.
[2] M. Soliman *et al.*, J. Radioanal. Nucl. Chem., **299** (2014) 89-93.
[3] H. Kikunaga, *et al.*, KURRI Progress Report 2013, PR10-3, (2014).
[4] Dinelli *et al.*, L. Geochem. Explor. 112 (2012) 54-75.

CO12-17 Neutron Resonance Spectrometry of Urinium for Nuclear Security and Safeguards Education

J. Kawarabayashi, H. Tagawa, Y. Ikeda, K. Mitsui and J. Hori[1]

Department of nuclear safety engineering, Tokyo City University

[1]Institute for Integrated and Nuclear Science,Kyoto University

INTRODUCTION: In order to support nuclear facility regulations in Japan for safe use, it is necessary to develop educational training course with broad knowledge associated with nuclear engineering. Nuclear facilities include reprocessing, nuclear fuel factories, research facilities, etc. in addition to nuclear power plants, it is important to teach not only the knowledge of radiation, reactor physics, but also the physics of nuclear material itself at each stage of the nuclear fuel cycle. The knowledge of physical and chemical properties of nuclear material is also needed for effective regulation. As a part of this human resource development, we propose an isotope ratio measurement training with uranium using pulsed neutron spectrometry as a candidate for the nuclear regulatory educational course to deepen the understanding of the nuclides in nuclear fuel cycle. Observation of the neutron resonance absorption phenomena of natural, enriched and depleted uranium will develop the understanding of the isotope itself and the properties of the nucleus of uranium. In this fiscal year, we conducted experiments to acquire neutron resonance absorption spectra of various samples including uranium in order to establish a procedure for practical training.

EXPERIMENTS: Natural Uranium oxide sample and some metal plates (Ag, Ta, etc.) were irradiated at KURRI-LINAC to record neutron transmission spectrum. A ^{3}He proportional counter followed by a multiple-stop time spectrometer (ORTEC EASY-MCS) was set just behind the sample at 13m experimental room and generated neutron detection signal. A signal from the accelerator was used as the start signal of the time spectrometer. The timing calibration between start signal and output signal of the ^{3}He proportional counter was performed with an oscilloscope by gamma-flash signal generated at the Ta target of the accelerator.

RESULTS: As shown in Fig.1, time spectrum with and without the natural uranium sample were obtained successfully with measurement of 20,000 sweeps and 21 m second range. The accelerometer was running in 50Hz Long mode, each spectrum was recorded within about 15 minutes. There were some resonance dips corresponding to ^{238}U while no dip of ^{235}U was observed. The cross section of resonance peak in ^{235}U is about one order lower than that of ^{238}U and the isotope ratio of ^{235}U to ^{238}U is about 0.71%, the dip intensity of ^{235}U would be three order lower than that of ^{238}U. The number of counted signal in one channel (i.e. 1 micro second) is in about as shown in Fig. 1, it would be necessary to record least one order of magnitude more signals to detect the resonance absorption of ^{235}U in this experiment. In Fig. 2, a resonance dip of ^{109}Ag was observed in the time spectrum with the sample of silver plate. The energy of this dip was estimated to be 5.25eV derived from the source-detector distance of 13m and dip position of 0.317 msec. The first energy level of ^{109}Ag is 5.19eV [1]. There is a good agreement between the experimental result and literature values.

CONCLUSION: We proposed pulsed neutron spectrometry as a candidate for the nuclear regulatory educational course to deepen the understanding of the nuclides in nuclear fuel cycle. The experimental results require at least acquisition period of 150 minutes to observe ^{235}U in natural uranium sample.

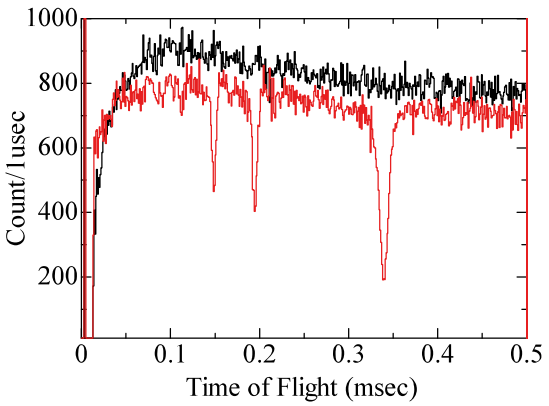

Fig. 1. Time spectrum of natural uranium sample (red). Black line is time spectrum of no sample. There are three dips corresponding to resonance absorption of ^{238}U.

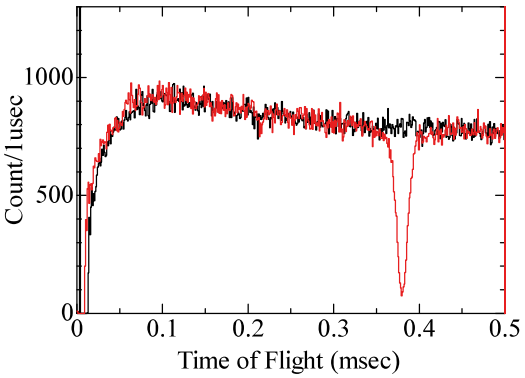

Fig. 2. Time spectrum of a silver plate sample (red). Black line is time spectrum of no sample. There is one dip at 0.317msec which is corresponded to resonance absorption of ^{109}Ag energy level of 5.25eV.

REFERENCES:

S. F. Mughabghab, Atlas of Neutron Resonances.

CO12-18 Evaluation test of SEL recovering system used in CubeSat by using ^{252}Cf

H. Masui, T. Murase, M. Cho, S. Wei[1], C. Joseph[1] and K. Takamiya[2]

Laboratory of Spacecraft Environment Interaction Engineering, Kyushu Institute of Technology

[1]*Nanyang Technological University*
[2]*Institute for Integrated Radiation and Nuclear Science, Kyoto University*

INTRODUCTION: Commercial-Off-The-Shelf (COTS) Integrated Circuits (ICs) are mostly sensitive to irradiations (e.g., protons, heavy-ions, etc.) in space, leading to various Single-Event Effects (SEEs). Among different SEEs, Single-Event-Latchup (SEL) is probably the most critical because it is detrimental and often damages ICs[1, 2]. This paper reports a circuit implementation that serves to provide protection for COTS ICs from SEL. Kyushu Institute of Technology (Kyutech) and Nanyang Technological University (NTU) are conducting a joint research program in 1U CubeSats project of BIRDS-4. In BIRDS-4 project, LDAP(Latch-up Detection and Protection) developed by NTU as a part of the mission of BIRDS-4[3] were installed (Fig. 1). LDAP monitors the latch-up current occurred in a device and shutdowns the power line of the device. The on-ground hardware verification on the basis of ^{252}Cf was demonstrated that the circuit successfully cuts off the SEL current and subsequently resets the COTS IC. The reported circuit has been adopted in a 1U CubeSat that will be launched early 2020.

EXPERIMENTS: Figure 2 shows the circuit diagram. In this test, an AD converter was adopted as a sample, and SEL was induced in the AD converter. A package of the AD convertor was removed(=de-caped) for radiation from ^{252}Cf. The AD convertor was set in the vacuum chamber and its pressure was less than 30 Pa. ^{252}Cf source was mounted on XYZ stage and the position of ^{252}Cf was controlled from outside and was moved above the sample. We checked whether LDAP can detect the SEL and can cut the power line connected the AD con-verter. To check the function of LDAP, the actual latch-up current was measured with a measuring instrument and the response of LDAP with a serial communication was monitored with PC1.

RESULTS: Figure 3 shows the current profile acquired with the measuring instrument. The current peak in the current profile shows the current increasing due to SEL. After the SEL, the current quickly recovered to the nominal current. This means that LDAP was able to detect the SEL in the AD convertor and to reset the power line of the AD convertor. In the same way, it was confirmed that the LDAP correctly worked with the serial communication. Since the LDAP function was confirmed, LDAP was installed on the mission board of the BIRDS-4 flight model. BIRDS-4 satellite will be launched in FY2020 and on-orbit demonstration will be planed.

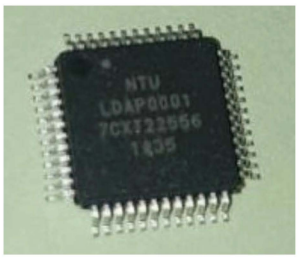

Fig. 1. LDAP (Latch-up Detection and Protection).

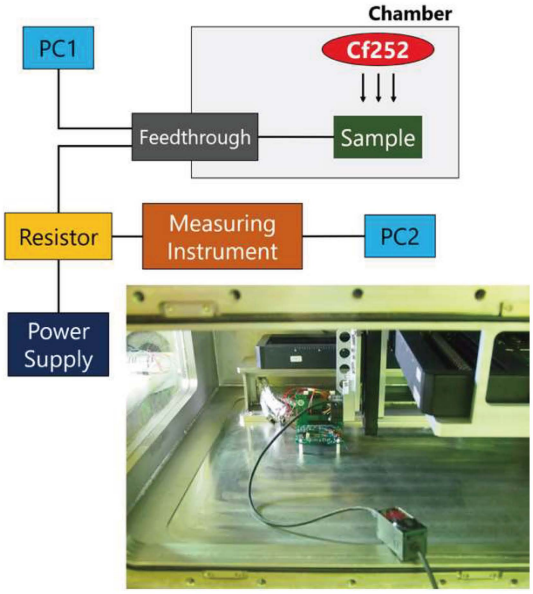

Fig. 2. Circuit diagram and phot of setup.

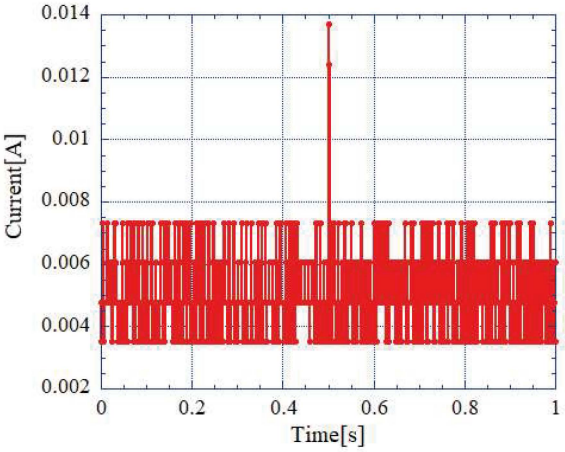

Fig. 3. Latch-up current detection and recovery.

REFERENCES:

[1] M. Cho *et al.*, "Test and Verification of Nanosatellite HORYU-II and Orbital Anomaly Investigation", Aerospace Technology Japan,12 17-24, 2013.
[2] Tomioka *et al.*, "Screening of nanosatellite microprocessors using californium single-event latch-up test results", Acta Astronautica, 126, 334-341, 2016.
[3] https://www.birds-project.com/